Ceramics-Silikáty 67 (1), 100-108 (2023)
www.ceramics-silikaty.cz doi: 10.13168/cs.2023.0007

AMOXICILLIN-LOADED HYDROXYAPATITE-ENRICHED SCAFFOLDS FOR DRUG RELEASE AND GUIDED BONE REGENERATION

#MUSTAFA SENGOR

Department of Metallurgical and Materials Engineering, Faculty of Technology, Marmara University, Istanbul, Turkey

#E-mail: mustafa.sengor@marmara.edu.tr

Submitted January 4, 2023; accepted February 7, 2023

Keywords: Hydroxyapatite, Bioceramics, Drug release, Porosity

The design of scaffolds for controlled drug release in bone tissue engineering requires careful consideration of several factors. Scaffold degradation and drug diffusion within the polymer matrix, influenced by pore size and distribution, must be carefully considered in the design of composite scaffolds. In this study, multi-functional scaffolds containing different amounts of hydroxyapatite (0, 0.25, 0.5, 1 % wt/wt) were prepared and characterised in terms of their chemical and morphological properties, as well as their drug release capabilities. Amoxicillin was used as a model drug to investigate the kinetic release model of the scaffolds, which were created using a freeze-dry method to form a spongy structure. Image processing techniques were used to measure the surface pore sizes and distributions. The results showed that the 0.5 wt. % hydroxyapatite-added scaffold had the smallest size, with an average pore size of 7 ± 4.3 μm and a weight loss of 45 %. All the prepared scaffolds fit Hill's kinetic model. The best fitting one was observed in the 0.5 wt. % addition. By carefully considering all the factors, it is possible to optimise the release of the drug from the polymeric material and the degradation characteristics to improve its performance.

INTRODUCTION

Guided bone regeneration (GBR) is a surgical technique used in oral and maxillofacial surgery to repair and regenerate bone in the facial region. It is often used to repair defects or deficiencies in the jawbone, which can occur due to various reasons, such as trauma, infection, or congenital abnormalities [1]. GBR involves the use of a membrane/scaffold to separate the bone defect from the surrounding tissue, allowing for the growth of new bone tissue in the defect area. The membrane acts as a physical barrier, preventing the ingrowth of soft tissue into the defect while allowing bone-forming cells (osteoblasts) to migrate into the area and regenerate the bone [2]. There are several advantages to using GBR in oral and maxillofacial surgery: improved aesthetics, enhanced function, increased stability, and reduced morbidity [3]. GBR is an important technique in oral and maxillofacial surgery that can improve the appearance and function of the jaw, as well as enhance the stability of dental implants.

Hydroxyapatite (HAp, $Ca_{10}(PO_4)_6(OH)_2$) is a calcium phosphate mineral that is found naturally in the human body and is the main component of human bones. It is an important material in guided bone regeneration as it is biocompatible with human tissues and has a low risk of causing an immune reaction. It has a high osteoconductivity and can act as a scaffold responsible for the migration and proliferation of bone-forming cells (osteoblasts), leading to the formation of new bone tissue [4].

HAp-based membranes/scaffolds can be grouped into three categories based on their composition: those that are coated with Hap [5], are reinforced with Hap [6], and are made entirely of pure Hap [7]. When choosing a membrane for use in guided bone regeneration, there are several key factors to consider, including its porosity (to allow for nutrient flow), degradation rate, cost, and mechanical properties.

There are a number of different polymers that have been used in combination with HAp in guided bone regeneration, including synthetic polymers such as polylactic acid and polyvinyl alcohol, as well as natural polymers such as gelatin and chitosan [8]. There are several advantages of natural, bio-degradable materials: being low-cost, and having recognitive structures, gelatin and milk proteins are widely used in bone tissue engineering [9]. Moreover, due to their structure that can

be dissolved in water under mild conditions, they can be easily processed. Casein is the most common protein in milk and sodium caseinate (NaC) is formed by precipitating acid-treated casein with alkaline. Sodium caseinate is used in combination with different materials in drug release due to its colloidal structure formed in water. Sodium caseinate can be used in combination with other bio-materials such as starch, cellulose, albumin, etc. to enhance the capabilities of the biomedical devices [10].

Maillard reaction is a type of reaction used to bind proteins to starch [11]. When combined with the Maillard reaction, starch and caseinate both become stable inside water and can be quickly gelled with protein cross-linking. In this way, one can indirectly bind starch while binding protein. For example, microbial transglutaminase (mTG) can cross-link caseinate and has no known toxic properties. mTG's microbial nature also lowers the production cost of enzymes compared to those obtained from animals and is greener than many other methods [12].

The materials used in tissue engineering must have additional properties beyond just containing biomaterials – they should also mimic the host tissue on a meso-scale in terms of their structure and shape [13]. Techniques, such as 3D printing and freeze drying, are used to create scaffolds with a porous structure, which is important for the transfer of liquids and the development of an extracellular matrix in 3D combined with homogenous cell distribution. Scaffolds can also be expected to facilitate drug delivery during treatment [14].

In this study, it was aimed to create degradable, 3D porous scaffolds by cross-linking sodium caseinate-starch-HAp composite scaffolds with mTG. The advantage of mTG not being damaged by freeze-drying and continuing to the cross-link afterwards was utilised. Prior to freeze-drying, the model drug amoxicillin was included inside the composite scaffold which is a common antibacterial drug used in the pharmaceutical industry. In this context, various analytical techniques were used to characterise the materials and evaluate their performance, including X-ray diffraction, Fourier transform infrared spectrum analysis, electron microscopy micrographs, calorimetric tests, degradation profiles, and UV spectroscopy.

EXPERIMENTAL

Materials and methods

NaC (Benosen, Turkey), starch (Merck, Germany), HAp (in powder form, Oerlikon Metco, Wohlen, Switzerland), and mTG (Tito in Istanbul, Turkey, 100 U/g), amoxicillin (MW 365.4 $g \cdot mol^{-1}$, Sigma-Aldrich, Germany) and phosphate-buffered saline (PBS, Sigma-Aldrich, Germany) were used in this study.

The scaffolds were prepared in parallel with the methodology of the previous work [15]. Deionised water at 70 °C was placed in each beaker, and 8 % (wt/wt) NaC and 8 % (wt/wt) starch were gradually added to prevent clumping. The solutions were slowly mixed with a magnetic stirrer at 60 rpm with a dish that covered the bottom of the cap. The protein-starch conjugate was formed gradually by the Maillard reaction for 5 hours, and the reaction was monitored by the colour change [11]. After the reaction, 0, 0.25, 0.5, and 1 % wt/wt of HAp was added to each solution. It was determined through the trial and error method that concentrations of hydroxyapatite (HAp) above 1 % caused high levels of precipitation and destruction of the polymer integrity. The solution was mixed for about 10 minutes at 70 °C and then allowed to cool to 40 °C. At the same temperature, amoxicillin was mixed into the solutions at a 1 % (wt/wt). Then, 4 % (wt/wt) of mTGs were added to the solutions. The solutions were left until the solution became gel-like. In this way, the precipitation of the HAp was prevented. The gel solutions were poured in a viscous state into cylindrical moulds measuring 10 × 40 mm, which were printed with a 100 % infill using a 3D printer. The samples were left in an incubator under water saturated conditions for 12 hours, and then kept at -20 °C for 2 hours. The samples were then placed in a freeze-drier, where they were kept at -50 °C for 12 hours and the liquid in the samples was sublimated and vapourised, resulting in porous 3D scaffolds. The composition of the raw materials and the identification (ID) of the sample groups in the solid samples are tabulated in Table 1. All the experiments were performed in triplicate at a minimum and the data are shown as means ± standard deviation (SD).

Table 1. Sample IDs and concentrations. Except for the powder case, all the materials were added in deionised water and the concentrations were with respect to the weight of the water.

Sample ID	Materials ratio (wt/wt)			Drug (% wt/wt)	Form
	Sodium Caseinate	*Starch*	*Hydroxyapatite*	*Amoxicillin*	
HAp	0.00	0.00	1.00	0.00	Powder
aHAp0	8.00	8.00	0.00	1.00	3D Scaffold
aHAp25	8.00	8.00	0.25	1.00	3D Scaffold
aHAp50	8.00	8.00	0.50	1.00	3D Scaffold
aHAp100	8.00	8.00	1.00	1.00	3D Scaffold
w/aHAp	1.00	1.00	0.00	0.00	3D Scaffold

Characterisation

The HAp peaks in the powder and 3D scaffolds were determined using an X-ray diffractometer (Shimadzu LabX XRD-6100). The tests were conducted between 10° and 60°, using Cu-Kα radiation source (λ = 1.54060 A), 40 kV, 30 mA, a sampling pitch of 0.02 degrees, and a speed of 2°/minute. The samples used in the test were prepared by smashing to a minimum size of 1 cm.

Fourier Transform Infrared Spectroscopy (FTIR) spectra were taken of the scaffolds using a JASCO-4000 Fourier Transform Infrared Spectroscopy. The spectra were taken over the wavelength range of 4000 to 500 cm^{-1} with a resolution of 2 cm^{-1}. The thermal characteristics of the scaffolds were examined using a differential scanning calorimeter (DSC-60 Plus, Shimadzu, Japan). Each sample was scanned from 25 °C to 300 °C at a heating rate of 10 °C·min^{-1}. The samples were placed in aluminium pans in amounts of around 5 mg. The y-axis of the graphs was normalised by weight.

In vitro degradation tests were performed in the PBS solution. Enzymatically crosslinked samples were divided into samples of around 50 mg, and their initial weights were recorded. The samples were put in plates and placed into an incubator at 37 °C for 7 days. At 24 hours intervals, measurements of the weights were performed, the samples were washed with deionised water and the solution was replenished. The percentage weight loss was calculated as

$$w_L\,\% = \frac{w_i = w_f}{w_i} \times 100,$$

where w_L % is the percentage loss and wi, wf are the initial and final weight of the samples, respectively.

Scanning electron microscopy (SEM, EVO LS 10, ZEISS) was used to inspect the size and morphology of the pores. The surface of the samples was sputter coated with gold/palladium to make the surface of the material conductive. The pore-sizes and porosity were measured with an image processing tool. A script was implemented through MATLAB software and images were imported for each sample groups. The image processing was semi-automatically conducted , based on the study of [16]. The operation was based on creating a depth map, a binary segmentation map, and a pore space segmentation map. The outputs were demonstrated in (Figure 4) and the average pore diameters with standard deviations are given in (Table 2 and Figure 5). Over 600 pore diameters were measured. To do this, the micron/pixel resolution was first set to 1.3, and the number of intensity levels was set to 4. The figures were first converted to grayscale. Then, a depth map was used to perform a depth analysis. The pores were then outlined in binary segmentation as black and white. The pore void and depth were illustrated with segmentation. Finally, the percentage of the porosity was determined from the ratio of the black area to white area. The pore diameters were calculated assuming that the calculated area was circular, using the formula √Area/π.

In order to evaluate the release properties of the amoxicillin from the hydroxyapatite (HAp) containing scaffolds, an *in vitro* drug release analysis was conducted. The scaffolds, each weighing approximately 5 mg, were placed in a 1 mL solution of PBS (pH 7.4 at 37 °C) and agitated on a rotary shaker at 250 rpm and 37 °C. Samples were taken at specific time points (at 0, 1, 2, 3, 4, 6, 18, 24, 48, 72, and 150 h) and 1 mL of the PBS solution was replaced with 1 mL of fresh PBS to continue the drug release test. The amoxicillin release profile was determined using UV spectroscopy (Shimadzu UV-3600, Japan) at 278 nm [17]. The used models with the formulas are given below:

0 order model: $Q = k \cdot t + Q_0$ (1)

1 order model: $Q = Q_0 \cdot e^{k \cdot t}$ (2)

Higuchi model: $Q = k \cdot \sqrt{t}$ (3)

Korsmeyer-Peppas model: $Q = k \cdot t^n$ (4)

Hill model: $Q = (Q_{max} \cdot t^n)/(k^n + t^n)$ (5)

In these equations, Q is the amount (%) of drug substance released at time t, Q_0 is the start value, Q_{max} is the maximum value of Q (100 %), t is the time, k-rate is a constant, n is the release exponent.

RESULTS AND DISCUSSION

Figure 1a displays the X-ray diffraction (XRD) pattern of the pure hydroxyapatite in powder form. The pattern exhibited the characteristic of low crystallisation apatite patterns. Characteristic peaks of HAp powder can be seen in Figure 1a. Polymeric 3D scaffolds were ground to a powder form and placed inside the aluminium plate of the X-ray device, where the images shown in Figure 1b were obtained. Upon comparison of aHAp100 and aHAp0, which differ only in terms of the hydroxyapatite content, the influence of the added ceramic became apparent. The peaks at 2θ = 26, 30 and 32° coincided with the peaks on the left in Figure 1a. The effect of the organic polymer casein and starch on the XRD pattern was demonstrated in the amorphous pattern, indicated a lack of crystallisation. In Figures 1a and 1b, the peak at 2θ = 15° is present and does not seem to be related to the material, but related to the background. The XRD patterns were identified using the Crystallography Open Database (COD) having the card number 00-721-7892 [18].

The FT-IR data of the crosslinked porous scaffolds in powder form were analysed, as shown in Figure 2a. The peak at 1020 cm^{-1} was caused by the symmetric and asymmetric stretching of $\upsilon_1\upsilon_3(PO_4)^{3-}$ [19]. Other peaks in this region were also caused by starch with CO and CC stretching with some COH contributions [20]. These

peaks were not significantly different from each other due to the formation of a conjugate structure with the Maillard reaction. The amide I and amide II absorption peaks at 1633 and 1516 cm^{-1}, respectively, came from NaC [21]. The ratio of the peak from amide I to the peak in amide II indicated the crosslinking structure, which was observed in all the groups except aHAp0. In aHAp0, there is no effect of this bond, and no bond type is found at this point in HAP. The peak at 1747 cm^{-1} was formed by the effect of amoxicillin and can be interpreted as the interaction between the amoxicillin, enzymes, and HAP [22], which affects the strength of the crosslinking [23]. This specific peak was particularly strong in the aHAp25 sample.

The calorimetric analyses are reported in Figure 2b. Unlike other analyses, the calorimetric responses of the different meta-structures during the process were analysed here. In addition to the DSC graphs of the four groups, three more sub-cases were plotted above the horizontal dashed line: i) a case just after the Maillard reaction (legend name: Maillard), ii) a case just after the enzymes were added and gelation was completed without the addition of HAp (legend name: FreezeDry), iii) a case after 12 hours of crosslinking in which there is no amoxicillin and HAp (legend name: w/aHAp).

The required heat is increased as the opportunity for the crosslinking increased. The melting temperature of the added amoxicillin and crosslinked normal groups was observed to be 271 °C for aHAp25 and aHAp100, and ~ 250 °C for aHAp0 and aHAp50. As the HAP content increased among the samples (amoxicillin-crosslinked groups), the enthalpy required for the denaturation of the proteins decreased. The temperature at which denaturation occurred, as detected by the highest point of the endotherm, was also shifted towards the left (65, 62, 61, 55 °C) with increasing the HAP (0, 0.25, 0.5, 1 %)

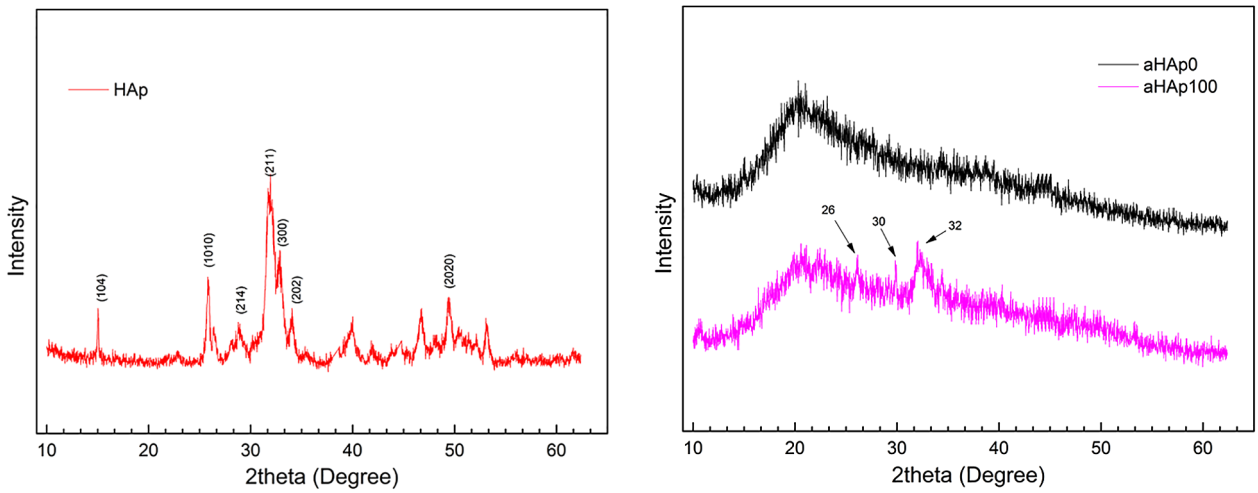

Figure 1. XRD pattern of: a) powder form hydroxyapatite (HAp), b) HAp free and 1 % wt/wt HAp added scaffolds.

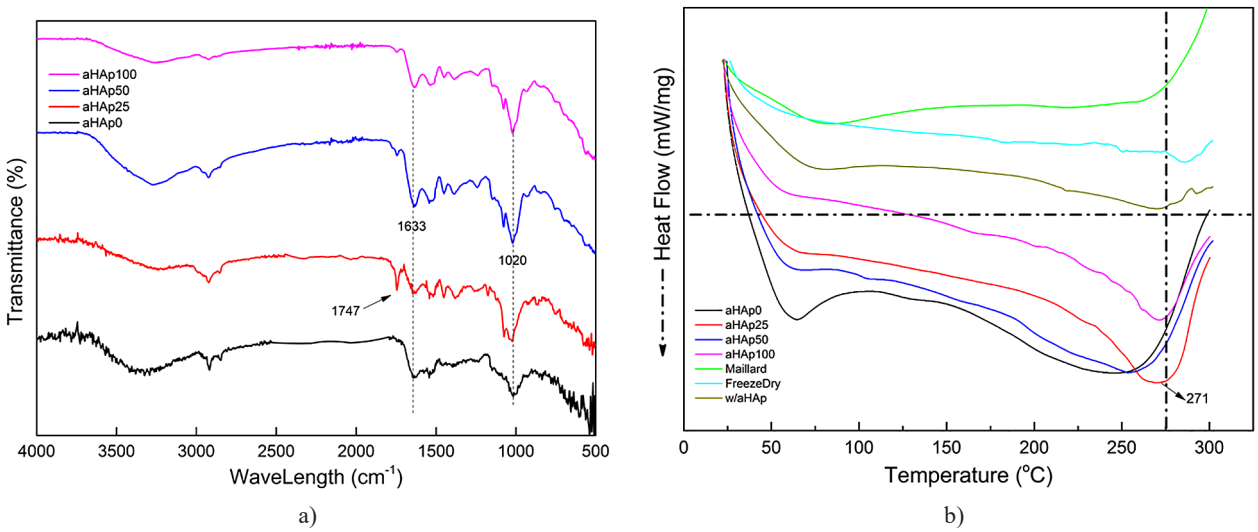

Figure 2. FT-IR spectroscopy (a) and DSC graphs (b) of the samples.

content (Figure 2b). The results of this study support the evidence in the literature demonstrating the impact of crosslinking on the denaturation temperatures [24]. At the melting point, the aHAp25 endotherm exhibited the biggest change in energy flow. The effect of the enzymatic crosslinking can also be observed at the melting temperatures. The melting temperatures of long cross-linked groups were shifted to the left during all 12 hours.

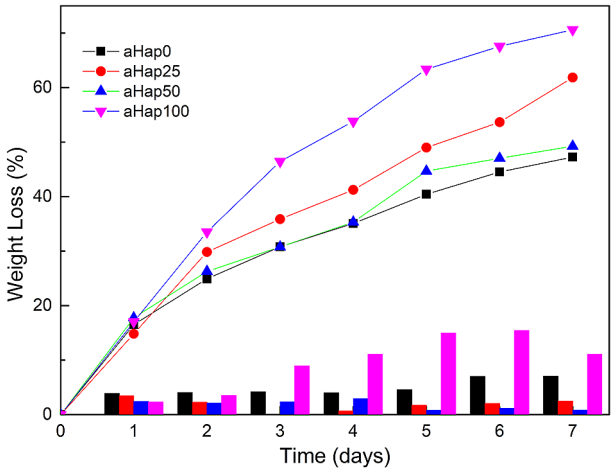

Figure 3. Degradation graphics of the porous, amoxicillin added scaffolds (The bars below indicate the standard deviations).

Upon analysing the degradation of the prepared groups, it was found that aHAp100 had the highest degradation, despite having a high standard deviation (Figure 3). This is thought to be due to the effect of hydroxyapatite ions which inhibit the transglutaminase enzyme activity. The group with the lowest crosslinking ratio had a high degradation (5^{th} day > 60 %), and the absence of ceramics in the crosslinking of the group (5^{th} day < 40 %) was more apparent in the degradation data. While all the groups had similar degradation profiles in the initial 24 hours, the differences widened in the subsequent days.

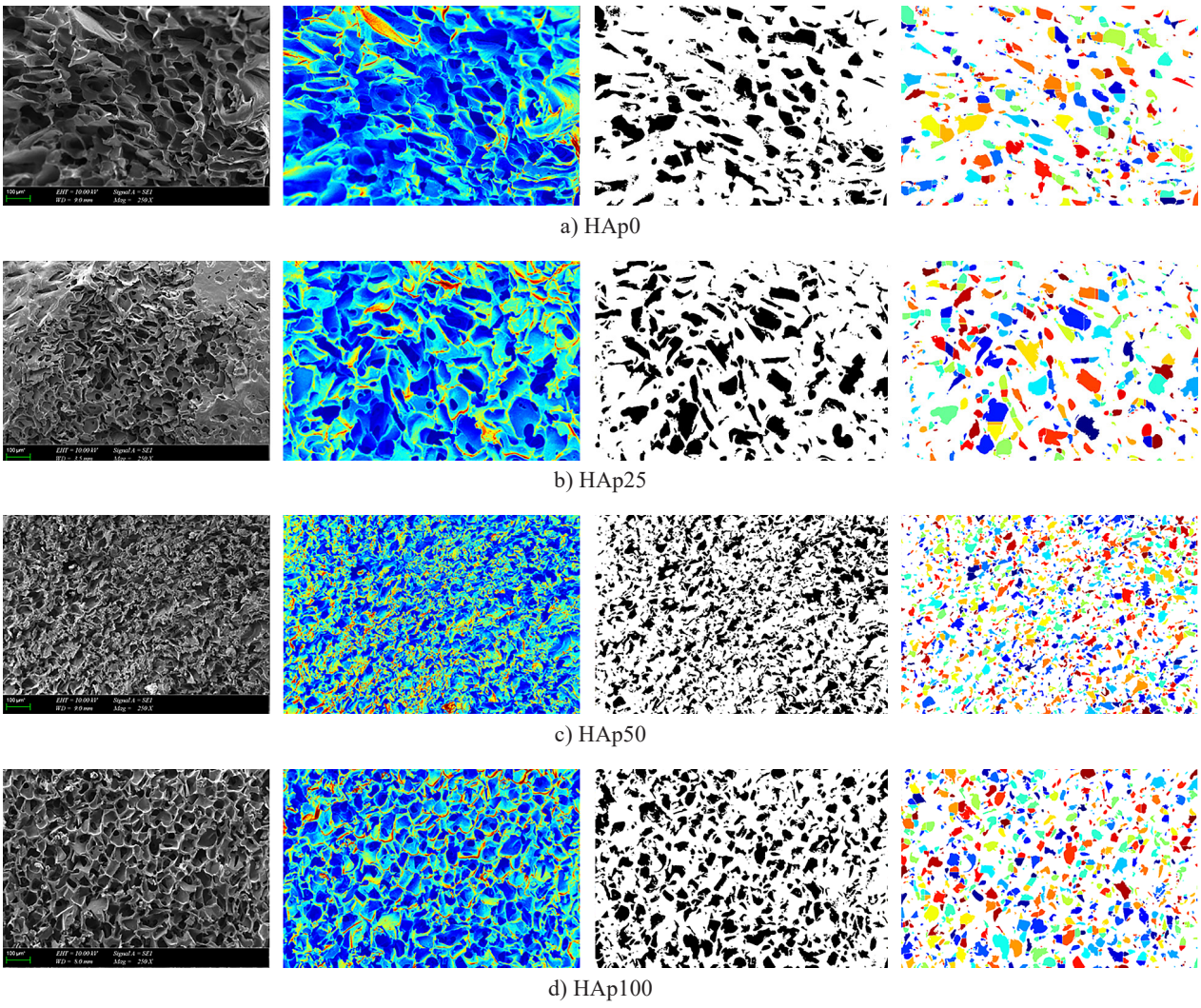

a) HAp0

b) HAp25

c) HAp50

d) HAp100

Figure 4. SEM micrographs of the samples obtained at 250X, scale bar 100 um. Columns from left to right: original SEM micrograph, depth map, binary segmentation map, and pore space segmentation map; Rows: a) aHAp0, b) aHAp25, c) aHAp50, d) aHAp100.

Table 2. Porosity and pore radius values obtained via image processing.

	aHAp0	aHAp25	aHAp50	aHAp100
Porosity (%)	23	25	29	31
Pore Radius (μm)	10.04 ± 7.92	11.29 ± 8.45	7.00 ± 4.33	9.54 ± 6.30

The original SEM images showed that the biggest difference was in aHAp25, as observed in Figure 4 in the first column. While the pores in all the other groups were homogeneously distributed, aHAp25 showed signs of erosion towards the corners of the surface. Even though aHAp100 was the weakest among the scaffolds kept in the saturated vapour for 12 hours to create suitable conditions for the crosslinking, the first signs of collapse were observed in aHAp25. In fact, the enzyme activity continued in the formed film layer due to this collapse, which may have slowed down the degradation by forming a stronger film layer. aHAp50 has the smallest pore sizes which can be detected under the depth and binary segmentation maps.

The group with the highest porosity is aHAP100, which was likely due to the low crosslinking leading to the sublimation of large amounts of water through vaporisation. The group with the lowest pore density is aHAp0, with a value of 23 %. When the pore sizes are examined, aHAp50 has the smallest average pore size with 7.00 um. The narrowest distribution of the pore sizes in all the groups was aHAp50, had a distribution of pore sizes with more than 80 % below 10 μm. The widest range of pore size distribution was observed in aHAp25 (Figure 5).

The drug release profiles of the four groups were examined over a period of 150 hours, as seen in Figure 6a. In the long term, aHAp50 showed the fastest release profile among the groups due to its homogenous distribution of small pore sizes and high porosity, which resulted in the largest surface area. During the first 6 hours of release, all the groups released more than 60 % of the amoxicillin. Of note, aHAp25 released more than 15 % of the total on average in the first hour, which was double than the other groups. Generally, the release in the first region continued in all the groups until 72 hours. After 95 % had been released, the remaining 5 % was released slowly.

There are various drug delivery systems available, and their release kinetics can vary depending on the appropriate model. For example, the zero order model is suitable for diffusion controlled release, the Korsmeyer-Peppas model is suitable for release by surface erosion, and the Hill models are suitable for limited diffusion and surface erosion [25]. Figure 7 shows the profiles estimated using the least squares method for the different models, and Table 3 also includes the values of the constants for the profiles.

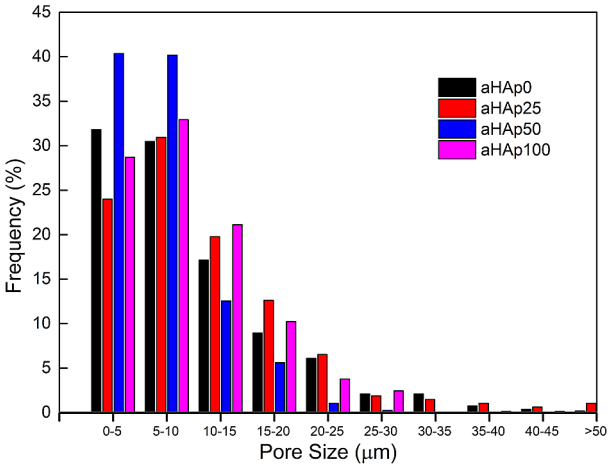

Figure 5. Pore Size distribution of the samples.

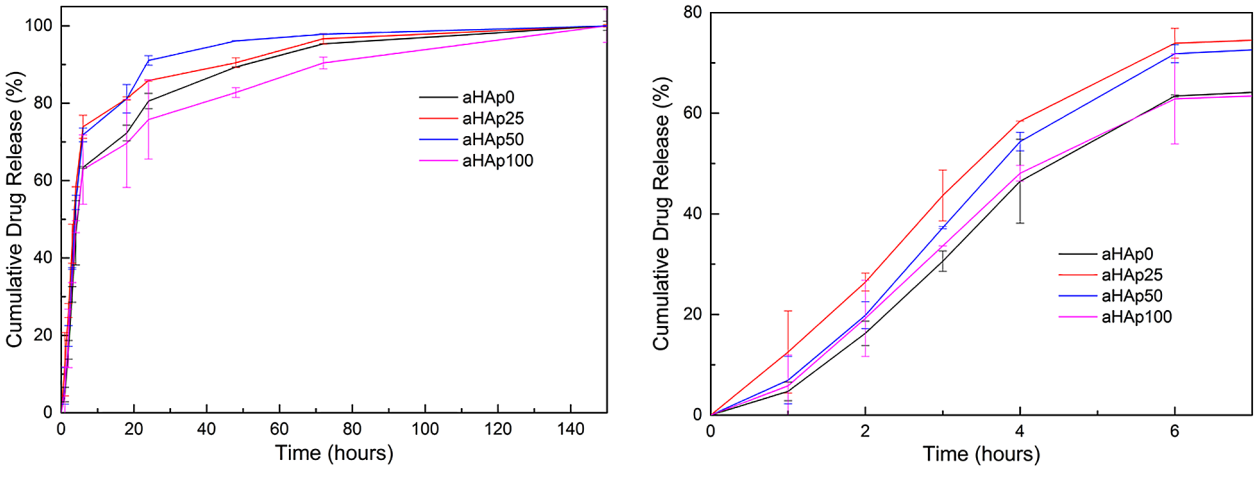

Figure 6. Amoxicillin release from the scaffolds a) long-term b) short-term.

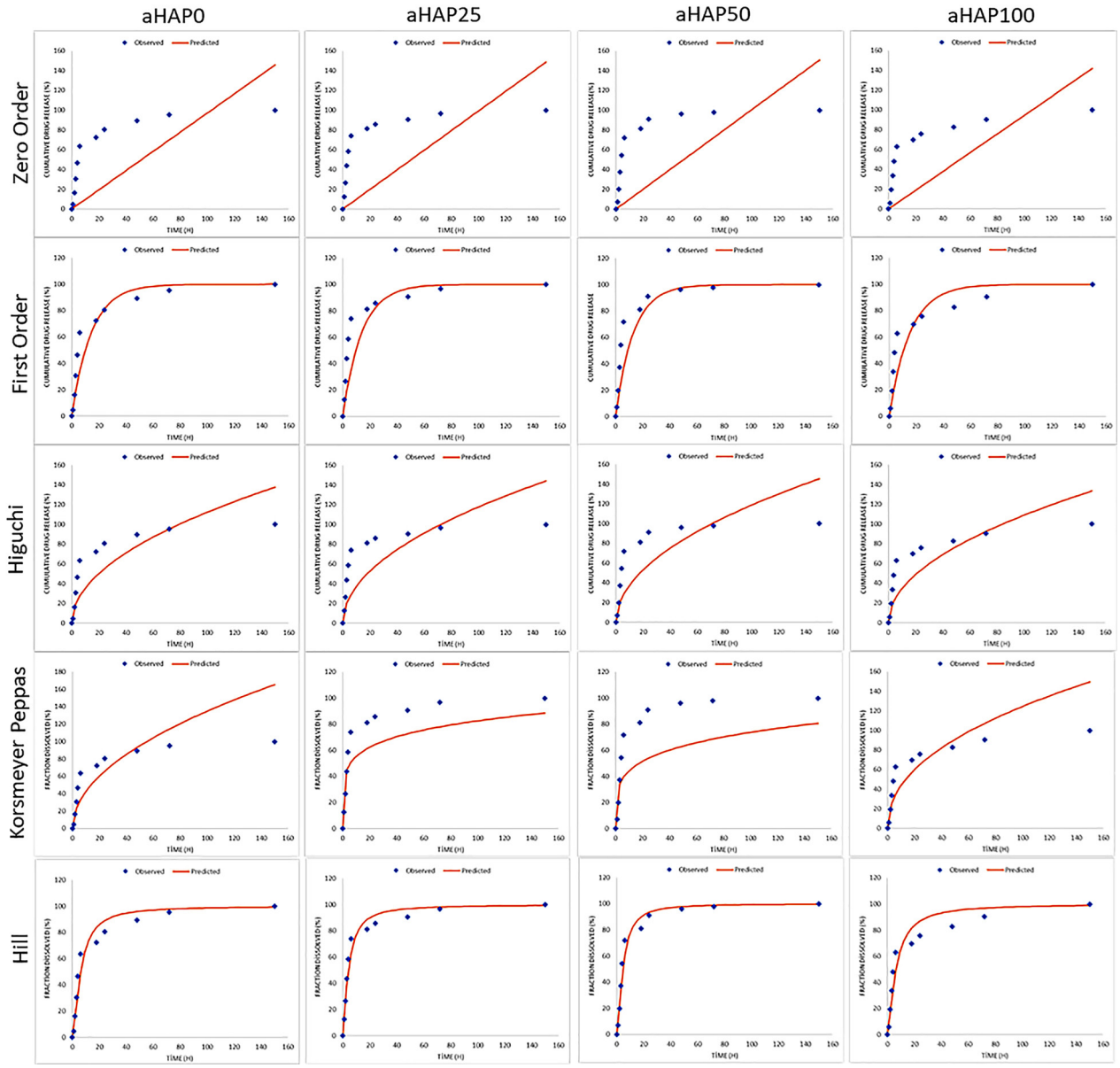

Figure 7. Drug release models observed vs the predicted plots.

Table 3. Constants of the selected models for all the samples.

Model name	Constants	aHAp0	aHAp25	aHAp50	aHAp100
Zero Order	k0	0.97	0.99	1.00	0.95
	R2	-0.25	-0.83	-0.55	-0.32
First Order	k1	0.07	0.07	0.08	0.07
	R2	0.88	0.71	0.83	0.82
Higuchi	kH	11.23	11.77	11.87	10.89
	R2	0.64	0.38	0.49	0.62
Korsmeyer-Peppas	kKP	13.37	37.03	26.62	15.46
	n	0.50	0.17	0.22	0.45
	R2	0.52	0.74	0.55	0.63
Hill	n	1.55	1.40	1.62	1.41
	K	16.90	7.41	12.00	13.30
	R2	0.89	0.88	0.94	0.82

It was found that the Zero order model was not suitable at all, while the First order and Hill models were suitable. In particular, the release characteristics of aHAp50 showed a strong fit to the Hill model, with an R^2 value of 0.94. The long-term release dynamics of the groups were similar, with aHAp50 exhibiting the fastest release due to its homogeneously small and numerous pore sizes, which results in small edges and a large surface area. The suitability of the Hill model also indicated that both the controlled diffusion and surface erosion are significant parameters in the release process.

In all the analyses, aHAp0 and aHAp50 gave values that were close to each other, while aHAp25 and aHAp100 also gave values that were close to each other. The calorimetric analysis of the HAp-free groups produced noteworthy results. The examination of the calorimetric properties of the HAp-free groups revealed that the melting point for the samples crosslinked through the enzymatic activity in the gel state was around 280 °C, whereas in the case of the full crosslinking (12 hours long) with enzymes, this temperature shifted towards 270 °C. If HAp and amoxicillin were added to the composition, the required energy difference increased. However, the main reason for this was actually the amoxicillin, as it was observed that the highest heat flow was in the case of aHAp0, where the HAp ratio was zero. The interaction between HAp and amoxicillin caused the crosslinking rate of the enzyme to vary between the groups. For example, the melting temperatures of aHAp25 and aHAp100 were close to the same point, and considering the 1747 cm^{-1} FT-IR peak, aHAp25 showed the highest amoxicillin specific bonds. The 0.25 % HAp ratio seemed to inhibit the interaction of amoxicillin with the matrix. The crosslinking efficiency was higher in the aHAp0 and aHAp50 groups, as indicated by the higher denaturation temperatures observed in these groups. The slowest degrading groups were again aHAp0 and aHAp50. The aHAp50 group had the lowest pore size of 7 microns and the second highest porosity of 29 %. With an R^2 of 0.94, this group was the most suitable for the Hill model, showing that both diffusion and surface erosion were more dominant than the bulk deformation.

It is possible that the addition of incremental amounts of HAp change the properties of the composite scaffolds in a non-linear manner due to the unique properties and interactions of each individual component. The addition of HAp may alter the distribution or arrangement of the other components within the scaffold, leading to changes in the overall physical and morphological properties of the protein and starch-based scaffolds. Additionally, the interactions between the different components of the scaffold, such as the transglutaminase, caseinate, starch, and amoxicillin, their concentrations, pH and temperature changes, the presence of certain functional groups or the overall conformations may also be affected by the addition of HAp, leading to further changes in the properties of the scaffold. It is known that amoxicillin can bind and chemically react with proteins [26]. This complex behaviour can be explained by the multiple interaction inside the composite scaffold.

CONCLUSION

In this study, amoxicillin-loaded, microbial transglutaminase-crosslinked, hydroxyapatite-enriched starch conjugated caseinate scaffolds were fabricated and characterised for their chemical and morphological properties as well as for their drug release capabilities. The optimal concentration of hydroxyapatite in the scaffold was determined through experimentation, with a 0.5 % concentration resulting in lower weight loss due to the non-linear interactions with the matrix, drug, hydroxyapatite, and enzyme. The surface pore size and porosity were optimal in the aHAp50 group, as determined through the image processing and analysis using MATLAB®. The drug release profiles followed Hill's kinetic model, indicating both diffusive and surface erosion release mechanisms. These scaffolds may have the potential for use in guided bone regeneration due to their ability to mimic the essential elements of the bone extracellular matrix.

Acknowledgement

The author would like to express gratitude to Oguzhan Gunduz and Bora Garipcan for their guidance, Fatih Serdar Sayin for the SEM analysis, and Merve Sirtikara for the kind support. This work is funded by the project Scientific Research Projects (FYL-2022-10436).

REFERENCES

1. Reichstein W., Sommer L., Veziroglu S., Sayin S., Schröder S., Mishra Y. K., et al. (2021): Initiated Chemical Vapor Deposition (iCVD) Functionalized Polylactic Acid–Marine Algae Composite Patch for Bone Tissue Engineering. *Polymers*, *13*(2), 186. doi: 10.3390/polym13020186
2. Alauddin M. S., Abdul Hayei N. A., Sabarudin M. A., Mat Baharin N. H. (2022): Barrier membrane in regenerative therapy: a narrative review. *Membranes*, *12*(5), 444. doi: 10.3390/MEMBRANES12050444
3. Sasaki J. I., Abe G. L., Li A., Thongthai P., Tsuboi R., Kohno T., Imazato S. (2021): Barrier membranes for tissue regeneration in dentistry. *Biomaterial Investigations in Dentistry*, *8*(1), 54-63. doi: 10.1080/26415275.2021.1925556
4. Le Thi B., Long B., Van Trung T., Van Thanh N. T., Ramesh S. (2022): Nanocrystalline hydroxyapatite prepared at different precursor concentrations: thermal stability, morphology and in vitro cellular response. *Ceramics-Silikaty*, *66*(1), 19-27. doi: 10.13168/CS.2021.0048
5. Jongprateep O., Jitanukul N., Saphongxay K., Petcharean-mongkol B., Bansiddhi A., Laobuthee A., et al. (2022):

Hydroxyapatite coating on an aluminum/bioplastic scaffold for bone tissue engineering. *RSC advances*, *12*(41), 26789-26799. doi: 10.1039/D2RA03285F

6. Kane R. J., Weiss-Bilka H. E., Meagher M. J., Liu Y., Gargac J. A., Niebur G. L., et al. (2015): Hydroxyapatite reinforced collagen scaffolds with improved architecture and mechanical properties. *Acta biomaterialia*, *17*, 16-25. doi: 10.1016/J.ACTBIO.2015.01.031
7. Tripathi G., Basu B. (2012): A porous hydroxyapatite scaffold for bone tissue engineering: Physico-mechanical and biological evaluations. *Ceramics International*, *38*(1), 341-349. doi: 10.1016/J.CERAMINT.2011.07.012
8. Ielo I., Calabrese G., De Luca G., Conoci S. (2022): Recent advances in hydroxyapatite-based biocomposites for bone tissue regeneration in orthopedics. *International Journal of Molecular Sciences*, *23*(17), 9721. doi: 10.3390/IJMS23179721
9. Khatun S., Appidi T., Rengan A. K. (2022): Casein nanoformulations-Potential biomaterials in theranostics. *Food Bioscience*, 102200. doi: 10.1016/J.FBIO.2022.102200
10. Şendil Ö., Samatya Yilmaz S., Yazici Ozcelik E., Uzuner H., Aytac A. (2022): Cross-linked electrospun polyvinyl alcohol/sodium caseinate nanofibers for antibacterial applications. *Journal of Vinyl and Additive Technology*. doi: 10.1002/VNL.21942
11. Consoli L., Dias R. A., Rabelo R. S., Furtado G. F., Sussulini A., Cunha R. L., Hubinger M. D. (2018): Sodium caseinate-corn starch hydrolysates conjugates obtained through the Maillard reaction as stabilizing agents in resveratrol-loaded emulsions. *Food Hydrocolloids*, *84*, 458-472. doi: 10.1016/J.FOODHYD.2018.06.017
12. Yang G., Xiao Z., Ren X., Long H., Qian H., Ma K., Guo Y. (2016): Enzymatically crosslinked gelatin hydrogel promotes the proliferation of adipose tissue-derived stromal cells. *PeerJ*, *4*, e2497. doi: 10.7717/PEERJ.2497/SUPP-6
13. Aghmiuni A. I., Keshel S. H., Sefat F., Akbarzadeh Khiyavi A. (2021): Fabrication of 3D hybrid scaffold by combination technique of electrospinning-like and freeze-drying to create mechanotransduction signals and mimic extracellular matrix function of skin. *Materials Science and Engineering: C*, *120*, 111752. doi: 10.1016/J.MSEC.2020.111752
14. Limongi T., Susa F., Allione M., Di Fabrizio E. (2020): Drug delivery applications of three-dimensional printed (3DP) mesoporous scaffolds. *Pharmaceutics*, *12*(9), 851. doi: 10.3390/PHARMACEUTICS12090851
15. Sengor M. (2022): Transglutaminase crosslinked sodium caseinate/starch/tri calcium phosphate based flexible sponge grafts. *Materials Letters*, *326*, 132943. doi: 10.1016/J.MATLET.2022.132943
16. Rabbani A., Salehi S. (2017): Dynamic modeling of the formation damage and mud cake deposition using filtration theories coupled with SEM image processing. *Journal of Natural Gas Science and Engineering*, *42*, 157-168. doi: 10.1016/J.JNGSE.2017.02.047
17. Salois A., Perez I., Palma E., Goolish E., Griko Y. (2015): Evaluation of the Chemical Integrity of beta-lactam antibiotics by iodine-based assay. *Journal of Biosciences and Medicines*, *3*(11), 91. doi: 10.4236/JBM.2015.311012
18. Altomare A., Corriero N., Cuocci C., Falcicchio A., Moliterni A., Rizzi R. (2015): QUALX2. 0: a qualitative phase analysis software using the freely available database POW_COD. *Journal of Applied Crystallography*, *48*(2), 598-603.doi: 10.1107/S1600576715002319
19. Gunduz O., Sahin Y. M., Agathopoulos S., Ben-Nissan B., Oktar F. N. (2014): A new method for fabrication of nano-hydroxyapatite and TCP from the sea snail Cerithium vulgatum. *Journal of Nanomaterials*, *2014*, 1-1.doi: 10.1155/2014/382861
20. Pozo C., Rodríguez-Llamazares S., Bouza R., Barral L., Castaño J., Müller N., Restrepo I. (2018): Study of the structural order of native starch granules using combined FTIR and XRD analysis. *Journal of Polymer Research*, *25*, 1-8. doi: 10.1007/S10965-018-1651-Y/METRICS
21. Zhao T., Liu F., Duan X., Xiao C., Liu X. (2018): Physicochemical properties of lutein-loaded microcapsules and their uptake via Caco-2 monolayers. *Molecules*, *23*(7), 1805. doi: 10.3390/MOLECULES23071805
22. Songsurang K., Pakdeebumrung J., Praphairaksit N., Muangsin N. (2011): Sustained release of amoxicillin from ethyl cellulose-coated amoxicillin/chitosan–cyclodextrin-based tablets. *Aaps Pharmscitech*, *12*, 35-45. doi: 10.1208/S12249-010-9555-0
23. Kumar B. S., Hemalatha T., Deepachitra R., Raghavan R. N., Prabu P., Sastry T. P. (2015): Biphasic calcium phosphate–casein bone graft fortified with Cassia occidentalis for bone tissue engineering and regeneration. *Bulletin of Materials Science*, *38*, 259-266. doi: 10.1007/s12034-014-0799-2
24. Orban J. M., Wilson L. B., Kofroth J. A., El-Kurdi M. S., Maul T. M., Vorp D. A. (2004): Crosslinking of collagen gels by transglutaminase. *Journal of Biomedical Materials Research Part A*, *68*(4), 756-762. doi: 10.1002/JBM.A.20110
25. Pham H., Ramos K., Sua A., Acuna J., Slowinska K., Nguyen T., et al. (2020): Tuning crystal structures of iron-based metal–organic frameworks for drug delivery applications. *ACS omega*, *5*(7), 3418-3427. doi: 10.1021/ACSOMEGA.9B03696/SUPPL_FILE/AO9B03696_SI_001.PDF
26. Yasmeen S., Rabbani G. (2017): Calorimetric and spectroscopic binding studies of amoxicillin with human serum albumin. *Journal of Thermal Analysis and Calorimetry*, *127*(2), 1445-1455.doi: 10.1007/S10973-016-5555-Y